Development, amplification, and decay of Atlantic/European summer weather patterns linked to spring North Atlantic sea surface temperatures

Article

Accepted Version

Development, amplification and decay of Atlantic/European summer weather patterns linked to spring North Atlantic sea surface temperatures

Albert Ossó[1,2], Rowan Sutton[2], Len Shaffrey[2] and Buwen Dong[2]

[1] Wegener Center for Climate and Global Change

[2] NCAS-Climate, University of Reading, Reading, United Kingdom

Corresponding author: Albert Ossó. Email address: albert.osso-castillon@uni-graz.at

Abstract

A recent study identified a relationship between North Atlantic SST gradients in spring and a specific pattern of atmospheric circulation in the following summer: the summer East Atlantic (SEA) pattern. It was shown that the SEA pattern is closely associated with meridional shifts in the eddy-driven jet in response to anomalous SST gradients. In this study, the physical mechanisms underlying this relationship are investigated further. It is shown that the predictable SEA pattern anomalies appear in June-July and undergo substantial amplification between July and August before decaying in September. The associated SST anomalies also grow in magnitude and spatial extent from June to August.

The question of why the predictable atmospheric anomalies should occur in summer is addressed, and three factors are identified. First is the climatological position of the storm track, which migrates poleward from spring to summer. Secondly, the magnitude of interannual SST variability underlying the storm track peaks in summer, both in absolute terms, and relative to the underlying mean SST gradient. The third factor is the most interesting. We identify a positive coupled ocean-atmosphere feedback, which operates in summer and leads to the amplification of both SST and atmospheric circulation anomalies.

The extent to which the processes identified are captured in the HadGEM3-GC2 climate model is also assessed. The model is able to capture the relationship between spring

Early Online Release: This preliminary version has been accepted for publication in *Journal of Climate*, may be fully cited, and has been assigned DOI 10.1175/JCLI-D-19-0613.1. The final typeset copyedited article will replace the EOR at the above DOI when it is published.

North Atlantic SSTs and subsequent ocean-atmosphere conditions in early summer, but the relationship is too weak. The results suggest that the real world might be more predictable than inferred from the models.

1. Introduction

The impact of the oceans on the large scale atmospheric circulation has received substantial attention from the climate forecasting community. Two-way air-sea interactions play a key role in tropical variability (e.g., Horel and Wallace 1981; Webster 1998), with the El Niño Southern Oscillation (ENSO) the most prominent example (e.g., Rasmusson and Wallace 1983; Philander 1983). At extratropical latitudes, the coupling between the atmosphere and ocean has generally been considered to be weaker than in the tropics (e.g, Kushnir *et al*. 2002 and references therein). However, new evidence suggests that the impact of the North Atlantic Ocean on the summertime extratropical atmosphere might be more important than previously thought. Gastineau and Frankignoul (2015) used a lagged maximum covariance analysis to investigate possible relations between North Atlantic SSTs and Euro-Atlantic atmospheric circulation. The authors found evidence that a large scale summer Z500 anomaly over the North Atlantic covaries with a precursor spring North Atlantic SST tripole pattern. Duchez *et al*. (2016) also presented evidence linking North Atlantic Sea Surface Temperature anomalies to the occurrence of European heat waves. In more recent work, Ossó *et al*. (2018) show evidence that the SST pattern reported by Gastineau and Frankignould (2015) is forced by anomalous atmospheric circulation during winter and spring, and that it then persists into summer when it influences the position of the jet stream in July-August (JA) by changing the background baroclinicity. The surface fingerprint of this jet displacement features an anomaly in sea level pressure (SLP) over the Northeast Atlantic, with its maximum centred west of the British Isles; the authors refer to this as the Summer East Atlantic (SEA) pattern. Ossó *et al*. 2018 showed that an index of North Atlantic SST in

March-April (MA) can predict the SEA pattern in July-August (JA) with a cross-validated skill of 0.67. The SEA pattern has a strong influence on rainfall over Ireland, the United Kingdom and North Western Europe, and it was shown that summer rainfall in this region can also be predicted with significant skill by a simple statistical model that includes the spring SST index as a predictor.

There is also evidence that summer atmospheric circulation in western Europe is subject to influences from the tropics. Wulff *et al*. 2017 show evidence that the second mode of summer low frequency variability in the Euro-Atlantic region is forced by diabatic heating anomalies, associated with tropical rainfall of opposing signs in the tropical Pacific and Caribbean. Coincidentally the authors described this mode also as the "Summer East Atlantic" (SEA) pattern. However, it is important to note that the SEA mode defined by Wulff *et al*. 2017 is different to that described by Ossó *et al*. 2018. O'Reilly *et al*. 2018 report that the dominant mode obtained from a Maximum Covariance Analysis between the summer Euro-Atlantic circulation and tropical precipitation features a cyclonic anomaly over the extratropical Atlantic, which resembles the Wulff *et al*. 2017 SEA pattern.

Dynamical seasonal forecast of European summer climate have until recently shown very little skill (e.g., Scaife *et al*. 2014; Arribas *et al*. 2011). However, a recent study by Dunstone *et al*. 2018 showed for the first time evidence of skilful dynamical predictions of European summer rainfall obtained using the latest high-resolution Met Office near-term prediction system. The authors show that the skill is linked to predictable North Atlantic SST variability which influences the supply of moisture over Europe and modulates convective rainfall. Despite representing important progress, this model has almost no skill in predicting the circulation variability, indicating that the model skill is primarily linked to thermodynamic processes. The results of Wulff *et al*. 2017, Ossó *et al*. 2018, and O'Reilly *et al*. 2018 therefore suggest that there is significant potential to improve the skill of dynamical seasonal forecasts by improving the fidelity which they can capture predictable dynamical (i.e. circulation)

signals. This opportunity motivates the need to better understand the processes that govern these signals, and to assess their representation in forecast models.

The purpose of this paper is to further investigate the predictable signals discussed in Ossó *et al*. 2018. Our primary aim is to identify and quantify the physical mechanisms that govern the intraseasonal evolution - from June to September - of the SEA pattern and its associated SST anomalies. In addition, we include a basic evaluation of the extent to which the mechanisms that operate in the real world are accurately simulated in the HadGEM3-GC2 global climate model used for seasonal forecasting at the UK Met Office.

The paper is organized as follows: Section 2 describes the data and the analysis techniques. In Section 3 we analyse the temporal and spatial evolution of the SEA pattern and associated SST anomalies, and the physical processes involved. In Section 4 we assess the ability of a global climate model (HadGEM3-GC2) to simulate the observed SEA pattern-SST relationship. Conclusions and implications are in Section 5.

2. Data and analysis techniques

We analyse monthly mean data from ECMWF Interim Reanalysis (ERA-Interim) (Dee *et al*. 2001). The analysis is performed on a 2.5^{o} x 2.5^{o} grid for the period 1979-2017 except if indicated otherwise in the figure captions. The regions where sea-ice concentration exceeds 1% are excluded from the SST field before analysis. To test the sensitivity of the results to the dataset used we have repeated the analysis using SLP data from HadSLP2 (Allan and Ansell 2006) and SST data from HadSST3 (Smith *et al*. 2008). The results do not change and all the conclusions stand the same. In Ossó *et al*. 2018 the SEA pattern is analysed using bimonthly mean anomalies. This choice is adequate to study the inter-annual variability of the pattern. Here however we are interested to investigate the intra-seasonal evolution of the SEA pattern during the summer months (from June to September) so monthly means are used instead. The data is linearly detrended to remove the influence of long-term

trends. Anomalies are calculated by subtracting the corresponding monthly climatology. In addition to the observational and reanalysis data, model simulation data from a 120 year preindustrial control run with the Met Office Global Coupled model 2.0 (HadGEM3-GC2) (Williams *et al*. 2015) is also analysed.

Ossó *et al*. 2018 identifies a North Atlantic pattern of covariability between SSTs and SLP and show that this pattern can be characterized with an SST index. The North Atlantic SST index (Fig S1) is calculated by averaging the March-April (MA) SST anomalies over the north-western box shown in Fig.1 (42°N–52°N; 52°W–40°W) minus the MA SST anomalies averaged over the south-eastern box (35°N–42°N; 35° W–20°W). The results are not sensitive to small variations in the region used to define the SST index. To be consistent with Ossó et al. 2018 we use MA mean SSTs to build the index. However, calculating the index using only March or April SSTs do not change the results. The SST index is standardized so it has a mean of zero and a standard deviation of one.

Linear regression and correlation analyses are performed to identify lead-lag linear relationships between variables. The statistical significance of the linear regression coefficients and correlations is estimated using a two-tailed Student's t-test with adjusted degrees of freedom to account for the autocorrelation of the time series following the methodology outlined in Santer *et al*. 2001.

The Eady growth rate is used as a measure of local baroclinic instability (Hoskins and Valdes 1990). The Eady growth rate is defined as $0.31(f/N)(du/dz)$, where f is the Coriolis parameter, N is the Brunt-Väisällä frequency, z is the vertical coordinate and u is the zonal wind. Storm track analysis is based on the tracking scheme developed by Hodges 1995, which identifies extratropical cyclones as 850-hPa relative vorticity maxima using 6 hourly data from the ERA-Interim reanalysis.

The monthly position of the jet core is identified in the 850-hPa monthly-mean wind field as the grid point with the wind speed maxima, identified using finite differencing. The

131 latitude of the JA mean North Atlantic eddy-driven jet is identified in the 850-hPa zonal wind
132 field following a method similar to that used in Woollings *et al*. 2010. First, the bimonthly zonal
133 wind at 850-hPa is zonally averaged between 0°-60° W over the North Atlantic. Then the
134 latitude of the maximum zonal wind between 20°-75°N is identified in the resulting time series.
135 Probability density functions (PDF) of the jet latitude climatology are calculated using a kernel
136 method (Deng *et al.* 2011). Jet latitude PDFs are also calculated for years with MA SST
137 index larger or smaller than plus one standard deviation (+1σ) or minus one standard
138 deviation (-1σ). The statistical significance of SLP and SST composites is tested by boot-
139 strapping with 1000 iterations the SLP and SST timeseries at each grid point.
140 Ocean mixed-layer temperature tendency is calculated by taking into account the
141 contributions due to surface radiation, surface turbulent fluxes and Ekman transport, using a
142 seasonally and spatially varying mixed-layer depth climatology from the French Research
143 Institute for Exploration of the Sea (De Boyer *et al*. 2004). For more details on the tendency
144 calculations see the methods section of Ossó *et al*. 2018.
145
146 **3. Observed development, amplification and decay of the ocean and atmospheric**
147 **anomalies**
148 **3.1. Evolution of SLP and SST anomalies**
149 Figure S1 shows the time evolution of the linearly detrended SST Index. During the
150 period considered in this study (1979- 2017) interanual variations dominate the SST Index.
151 A more detailed study of the temporal evolution of the SST Index is shown in the
152 complementary information of Ossó et al. 2018.
153 We analyse the evolution of ocean and atmospheric anomalies associated with the MA SST
154 index by performing a lagged linear regression analysis between monthly (from June to
155 September) SLP and SST anomalies with the precursor MA SST dipole index (Fig.1). The
156 SST regression coefficients in Figure 1 indicate the evolution of the SST field. In June, they

exhibit a dipole pattern that strongly resembles the precursor SST dipole in spring except the anomalies are weaker (compare Ossó et al. 2018, Fig.2). In July and August, the warm SST anomaly east of Newfoundland intensify and expand northeastward. In September and October, the warm anomaly starts to dissipate and by November, the anomaly magnitude is only about a quarter of that in August and the regression coefficients are no longer statistically significant (not shown).

The SLP regression coefficients indicate the evolution of the atmospheric circulation. Note that since the typical persistence time of the extratropical atmosphere is less than 1 month, large and statistically significant SLP regression coefficients in Fig. 1 suggest an atmospheric response to the underlying ocean. In June, a dipolar pattern of SLP anomalies extends across the North Atlantic, with an anticyclonic anomaly located over Western Europe and northeast Atlantic. In July, a stronger anticyclonic anomaly is centred over the central–east Atlantic. In August, this anticyclonic anomaly intensifies further, in terms of both magnitude and correlation with the preceding MA SST index (Fig. S2); its centre of action is also displaced slightly eastward. In September, the anticyclonic anomaly is no longer present and the anomalies are generally weak and not statistically significant.

3.2 Physical mechanisms

Ossó *et al*. 2018 showed that the SEA pattern is the surface fingerprint of North Atlantic jet stream fluctuations forced by changes in baroclinicity associated with the anomalous spring SST gradient. Here we explore the intraseasonal (June to September) jet variations (Fig. 2a, 2c, 2e and 2g) and Eady growth rate anomalies (Fig. 2b, 2d, 2f and 2h) linearly associated with the MA SST index. The regression pattern shows that June is characterized by weak westerly anomalies poleward of the climatological jet and weak easterly anomalies on its equatorward side. Positive and negative Eady growth rate anomalies are also apparent respectively poleward and equatorward of the jet but these are

183 weak and not statistically significant. In July and August, a similar pattern of zonal wind
184 anomalies is apparent but now the anomalies are substantially larger. There are, as well,
185 concurrent strong positive Eady growth rate anomalies (with a size of about 30% the
186 climatological value) poleward of the jet and slightly weaker negative anomalies (about 20%
187 the size of the climatology) on its equatorward side. The Eady growth rate anomalies are
188 forced by the anomalous SST meridional gradient (figure not shown) and are co-located with
189 the jet core anomalies shown in figure 2. This suggests a possible causality from the latter to
190 the former. However, the same jet anomalies might also force secondary Eady growth rate
191 downstream. Finally, in September the pattern of zonal wind and Eady growth rate anomalies
192 reverses; however, the anomalies are weak and not statistically significant.

193 Another perspective is obtained by examining the North Atlantic storm track itself, i.e.
194 the paths and other characteristics of extratropical cyclones. Figure 3 shows the regression
195 of JA storm track density (Fig.3a) and storm genesis density (Fig.3b) onto the MA SST index.
196 Figure 3a shows – consistent with Fig 2 - that a positive MA SST index is associated with a
197 poleward shift of the summer jet, with a ~30% density increase South-West of Iceland and a
198 ~30% density decrease east of the UK relative to the JA climatology. There are also changes
199 in the genesis density. Fig.3b shows an increase in genesis density south-east of Greenland
200 and East of Iceland, and a decrease west of the British Isles. The genesis density anomaly
201 south-east of Greenland could be associated with increased Greenland Tip Jet events
202 (Moore and Renfrew 2005; Harden et al. 2011; Harden and Renfrew 2012) due to the
203 favourable conditions associated with the northward displaced jet.

204

205 *Why should the atmospheric response to the underlying SST – involving the storm*
206 *track and eddy-driven jet – be strongest in July and August?*

207 Ossó *et al*. 2018 hypothesised that the timing of the atmospheric response may be
208 partly a consequence of the seasonal migration of the North Atlantic eddy driven jet. Here

209 we present evidence that both the seasonal migration of the jet *and* the seasonal evolution
210 of the SST variability contribute to explaining why the atmosphere responds primarily during
211 the summer months.

212 Figure 4 shows the seasonal variation of the eddy-driven jet latitude (see section 2).
213 In spring the jet is located south of the anomalous SST gradient measured by our SST index,
214 but in summer (from June to September) the jet is located over the region where significant
215 fluctuations in the SST gradient arise. These SST fluctuations are associated with
216 fluctuations in the Eady growth rate as shown in Figure 2 (d and f). Further insight is provided
217 by Figure 5, which illustrates the seasonal variation in both the mean (i.e. climatological) and
218 anomalous (due to interannual variability) SST gradient in the region measured by our index.
219 Fig.5a shows that the climatological SST gradient in this region declines rapidly in July and
220 August, whilst Fig.5b shows that the standard deviation is maximum in the same summer
221 months. Thus the ratio of these two quantities (i.e. standard deviation divided by mean SST
222 gradient index), shown in Fig.5c, shows a very strong peak in July and August. Based on
223 these results we hypothesise that the storm track may be particularly sensitive to variations
224 in the underlying SST gradient, which are about 15% of its mean value.

225 Overall our findings so far suggest two reasons for a strong atmospheric response in
226 summer:

227 (i) The storm track is located further north (Fig 4) in a region where there is
228 significant interannual SST variability;

229 (ii) The magnitude of interannual SST variability in this region peaks in summer,
230 both in absolute terms (Fig 5b) and relative to the underlying mean SST
231 gradient (Fig 5c), which is weaker in summer (Fig 5a).

232

233 **3.3 Amplification by ocean-atmosphere coupling**

234 Figure 5b shows that the variance of the SST index increases in summer, and Figs 1

and S2 show that this increase does not simply reflect additional uncorrelated summer variance ("noise") but rather that the magnitude, spatial extent and correlation of the SST variability that is correlated with the MA SST index also increases from June to July and July to August. This finding is surprising, as one would normally expect correlation in particular to decline with lead time. Ossó *et al*. 2018 suggested that this interesting behaviour might be explained by the existence of a positive ocean-atmosphere feedback which amplifies SST and SLP anomalies during the summer months. Here we investigate this hypothesis further.

Figure 6 analyzes the physical processes driving the evolution of the SST anomalies during June-September associated with the MA SST index. Figure 6a, 6d and 6g show the month-to-month change of the SST anomalies; Figure 6b, 6e and 6h show the total mixed layer temperature tendency and Figure 6c, 6f and 6i show the mixed layer temperature tendency due to radiation alone. Note that all three fields are regressed onto the MA SST index. SSTs in the central North Atlantic warm from June to July and from July to August. Detailed examination of the individual processes contributing to the mixed layer temperature tendency (see section 2) shows that the warming is forced by enhanced surface radiation and turbulent fluxes, while anomalous Ekman transports play a minor role. The contribution from increased surface radiation is particularly important for the warming between July and August (Fig 6f) and is associated with a reduction in cloud cover (not shown). The surface flux anomalies implied by Fig 6 arise in response to surface winds and cloud conditions associated with the anticyclonic SEA pattern anomalies shown in Fig 1. But we have already seen that the circulation anomalies themselves amplify, particularly between July and August. Thus our findings support the hypothesis of Ossó *et al*. 2018 that there is a positive coupled ocean-atmosphere feedback that operates over the North Atlantic Ocean in summer time, and provide further insight into the mechanisms involved: SST anomalies east of Newfoundland excite a circulation response which leads to amplification and eastward spread of the SST anomalies, and we hypothesise that also leads to concurrent amplification

261 of the atmospheric circulation anomalies. Note however, that the causality of this last step,
262 the concurrent amplification of the atmospheric anomalies, cannot be inferred from statistical
263 analysis alone since there is no lag between 'concurrent' anomalies. Further analysis (e.g.
264 model experiments) may be required to full identify all the steps in the positive feedback. The
265 SST anomalies grow primarily through the influence of turbulent and radiative surface heat
266 fluxes that directly associated with the anomalous atmospheric circulation. The role played
267 by surface radiation and associated cloud changes is especially interesting since it
268 represents a distinctive characteristic of summer mid-latitude air-sea interactions. This
269 coupled ocean-atmosphere amplification is an important additional reason for the strong
270 atmospheric response in summer.

271 From August to September the SST anomalies cool (Fig 6g) as the atmospheric
272 circulation anomalies also dissipate (Fig 1d). Analysis of the terms contributing to the mixed
273 layer temperature tendency shows that the cooling is largely dominated by anomalous
274 turbulent heat loss associated with the strengthening of the westerlies at around 45° latitude
275 from August to September (Figs 6 h and i).

276

277 **3.4 Evidence of nonlinearities**

278 So far we have analyzed the linear relationship between the atmosphere circulation
279 and the spring SST gradient. In this section we investigate whether there is evidence for any
280 nonlinear aspects to this relationship. Figure 7a compares the Kernel density distribution of
281 the eddy-driven jet latitude climatology (Woollings et al. 2010) with the distribution for years
282 with large positive and negative values of MA SST index ($> +1\sigma$ and $<-1\sigma$ respectively). For
283 positive values of the MA SST index the jet distribution is clearly skewed poleward compared
284 with the climatology while for negative values the distribution is only slightly displaced
285 equatorward. The asymmetry between these distributions does indeed suggest a nonlinear
286 jet response to the MA SST index. We have repeat the analysis of figure 7 using daily zonal

wind data instead of bimonthly means (figure not shown). The distributions are very similar and the qualitative results do not change. Further insights can be obtained from a composite of U850 anomalies (Fig.7c and 7d). The U850 anomalies for years with positive values of MA SST index are substantially larger than for years with negative values, again suggesting a nonlinear jet response to the SST anomalies.

Evidence suggests that the nonlinear character of the atmospheric anomalies may result from asymmetries in the SST dipole forcing in July. Figure 8 shows July composites of SSTs (Fig. 8a and 8b), cloud cover (Fig. 8c and 8d) and radiation flux anomalies (Fig. 8e and 8f). Comparison of Figs 8a and 8b shows that large positive values of the MA SST index (> +1σ) are associated with a much clearer dipole pattern than is the case for negative values of the index. However, there is also a role for changes in cloud cover and surface radiation, as shown by Figs 8c and e. Changes in cloud cover and surface radiation also occur in association with large negative values of the MA SST index (Figs 8d and f), but these changes are noisier over the subtropical region than is the case for positive values of the SST index.

Overall the evidence is that large positive values of the MA SST index excite the strongest atmosphere-ocean response in summer.

4. Representation of the SEA pattern - spring SST relationship in HadGEM3-GC2

The evidence from Osso et al 2018 and Section 3 of this paper suggests that the relationship between spring North Atlantic SST anomalies and the summer atmospheric circulation is an important source of predictability for European summer climate. It is therefore important to assess whether this relationship is captured in climate models used for seasonal forecasting. Here, we analyze the representation of this relationship in a 120-year long control simulation from the Met Office HadGEM3-GC2 model, which has an atmosphere horizontal resolution of N216 (about 60km at midlatitudes) and an ocean

313 resolution of 0.25° (Williams et al. 2015). We start by performing a MCA between the MA
314 mean SSTs and the JA mean SLP of the model (Fig.S3). Figure S3 shows a pattern of SST
315 anomalies in MA that covaries significantly with an SEA-like SLP anomaly in the subsequent
316 JA. The spatial pattern of SST and SLP anomalies is very similar to that obtained by applying
317 MCA to observational data (see Ossó et al. 2018, c.f., Fig.S1). Figure 9 shows the regression
318 patterns of SST and SLP anomalies onto an index representative of the HadGEM3-GC2 MA
319 SST dipole. U850 anomalies are shown in Fig.10. (Note that using an SST index defined as
320 for the observations does not change these results significantly.)

321 SLP and U850 anomalies for July are consistent with a statistically significant
322 atmosphere response to MA SSTs. The spatial patterns of SLP and SST anomalies are very
323 similar to that seen in observations but the magnitude of anomalies is about half. In August,
324 the contrast is much greater. The SLP anomalies are not statistically significant and the
325 U850 anomalies are barely so. The SST anomalies are also very weak. Whereas in the
326 observations we saw a rapid amplification of the ocean and atmosphere anomalies, in the
327 HadGEM3-GC2 model the anomalies decay. This evidence suggests that HadGEM3-GC2 is
328 able to capture the relationship between spring North Atlantic SSTs and subsequent ocean-
329 atmosphere conditions in early summer, but the relationship is weaker than is observed and
330 the model fails to simulate the positive feedback mechanisms that lead to rapid amplification
331 of the signal between July and August. These findings highlight important opportunities for
332 improving the HadGEM3-GC2 model, with a strong expectation that such improvements
333 would be beneficial for summer seasonal forecasts.

334

335 **5. Conclusions and implications**

336 In this study we have investigated the physical mechanisms that underpin the
337 relationship identified in Ossó et al. 2018 between a dipolar pattern of spring (March-April,
338 MA) North Atlantic SST anomalies and anomalous atmospheric circulation (particularly

339 associated with the SEA pattern) in the subsequent summer. We have examined the
340 development, amplification and decay of the SST and atmospheric anomalies, with a
341 particular focus on ocean-atmosphere interactions. Key findings are as follows:
342
343 • Ossó *et al*. 2018 identified a predictable July-August pattern of atmospheric circulation
344 in the North Atlantic (the SEA, Summer East Atlantic pattern) . More detailed analysis
345 in this study has shown that these anomalies appear in June-July and undergo
346 substantial amplification between July and August before decaying in September. The
347 associated SST anomalies also grow in magnitude and spatial extent from June to July
348 and July to August.
349 • Monthly analysis further supports the evidence presented by Ossó *et al*. 2018 that the
350 SEA pattern response is a consequence of meridional shifts in the summer storm track
351 and associated eddy-driven jet in response to the SST anomalies. These shifts are
352 closely associated with changes in the Eady growth rate and the underlying meridional
353 SST gradient.
354 • There are also changes in the storm track genesis density associated with the SST
355 gradient. In particular, the reduction of the genesis density over the Southern SST index
356 box is consistent with the observed poleward displacement of the storm track.
357 • An important question is why should the predictable atmospheric anomalies occur in
358 summer (specifically July-August)? We have identified three factors:
359 (i) In comparison to spring, the storm track and associated eddy-driven jet are
360 located further north in a region where there is significant interannual SST
361 variability.
362 (ii) The magnitude of interannual SST variability in this region peaks in summer,
363 both in absolute terms, and relative to the underlying mean SST gradient, which
364 in summer is weak.

(iii) As hypothesized by Ossó *et al*. 2018, a positive coupled ocean-atmosphere feedback operates in summer, which leads to the amplification of both SST and atmospheric circulation anomalies, and is particularly effective between July and August. Amplification of the SST anomalies is caused primarily by anomalous surface turbulent and radiative fluxes; the latter are associated with changes in cloud cover. The enhanced SST anomalies increase the anomalous baroclinicity and thereby excite a stronger atmospheric response. This positive ocean-atmosphere feedback sustains and amplifies the SEA pattern in July and August.

- The SST and SEA pattern anomalies decay in September. The SST anomalies are damped by turbulent surface fluxes.
- There is evidence that the summer atmospheric response to SST anomalies is nonlinear. Large positive values of the MA SST index excite the strongest atmosphere-ocean response in summer. The summer atmospheric response is characterised by a substantial poleward shift in the North Atlantic eddy-driven jet. The associated summer SST anomalies feature positive anomalies across the mid-latitude anomalies extending east from Newfoundland, with negative anomalies in the eastern subtropical Atlantic.
- A global climate model, HadGEM3-GC2, is able to capture the relationship between spring North Atlantic SSTs and subsequent ocean-atmosphere conditions in early summer, but the relationship is weaker than is observed and the model fails to simulate the positive feedback mechanisms that lead to rapid amplification of the signal between July and August.

Recent research on the potential drivers of summer Euro-Atlantic climate suggests that the predictable component of summer atmospheric circulation at seasonal timescales may be larger than previously thought. As discussed in the Introduction, both tropical precipitation [e.g., Wulff *et al*. 2017, O'Reilly *et al*. 2018] and extratropical SST gradients

391 [Gastineau and Frankingnoul 2015, Duchez *et al.* 2016, Ossó *et al*. 2018 and this study] have
392 shown potential as predictors of the summer Euro-Atlantic climate. Furthermore, recent work
393 by Dunstone *et al*. 2018 shows evidence of skillful seasonal forecasts of summer rainfall over
394 Europe using the latest high-resolution Met Office seasonal prediction system. However, the
395 skill of these predictions is primarily linked to thermodynamic processes - there is insignificant
396 skill for atmospheric circulation - and the magnitude of the predicted signals is much smaller
397 than in the real world. These features are a manifestation of the so-called "signal-to-noise
398 paradox" (Scaife and Smith 2018) which was first identified in seasonal forecasts for
399 European winters (Scaife *et al*. 2014). In this study, we have shown that a key physical
400 process shaping the predictability of Atlantic/European summers - amplification through
401 coupled ocean-atmosphere feedback - is not well represented in the HadGEM3-GC2 model
402 (which is very similar to the model used for seasonal predictions by Dunstone *et al*. 2018).
403 This implies that this weakness could be an important factor in accounting for the signal-to-
404 noise paradox in summer seasonal forecasts (Dunstone *et al*. 2018). Investigating the
405 reasons for the model weaknesses in this regard – for example whether they are due to poor
406 representation of SST-cloud-radiation feedbacks or other processes – will be an important
407 area for future work. It will also be important to evaluate other climate models, especially
408 those used for seasonal predictions, to assess the extent to which the mechanisms we have
409 identified are accurately simulated.
410
411 **Acknowledgements:** This work was supported by SummerTIME project funded through the
412 Natural Environment Research Council (NERC) "Drivers of variability in atmospheric
413 circulation" programme. AO, LS, BD and RS are supported by the U.K. National Centre for
414 Atmospheric Science (NCAS) at the University of Reading.
415
416 **References**

Allan, R., and T. Ansell, 2006: A new globally complete monthly historical gridded mean sea level pressure dataset (HadSLP2): 1850–2004, *J. Climate*, **19**, 5816 – 5842.

Arribas A, *et al*., 2011: The GloSea4 ensemble prediction system for seasonal forecasting, *Mon. Wea. Rev*. **139**, 1891–1910.

Dee, D. P., S.M. Uppala, A. J. Simmons, P. Berrisford, P. Poli, S. Kobayashi, ... &P. Bechtold, 2011: The ERA-Interim reanalysis: Configuration and performance of the data assimilation system, *Q. J. R. Meteorol. Soc*, **137**, 553 – 597.

Deng, H., H. Wickham, 2011: Density estimation in R. Electronic publication.

Duchez, A., et al., 2016: Drivers of exceptionally cold North Atlantic Ocean temperatures and their link to the 2015 European heat wave. *Environmental Research Letters* 11.7: 074004.

Dunstone, N., D. Smith, A. Scaife, L. Hermanson, D. Fereday, C. O'Reilly, *et al*., 2018: Skilful seasonal predictions of summer European rainfall, *Geophys. Res. Lett*., **45**, 3246–3254. https://doi.org/10.1002/2017GL076337.

Gastineau, G., and C. Frankignoul, 2015: Influence of the North Atlantic SST variability on the atmospheric circulation during the twentieth century, *J. Climate*, **28**, 1396 – 1416.

Harden, B. E., I. A. Renfrew, and G. N. Petersen, 2011: A Climatology of Wintertime Barrier Winds off Southeast Greenland. J. Climate, 24, 4701-4717.

442 Harden, B. E., and I. A Renfrew, 2012: On the Spatial Distribution of high winds of southeast
443 Greenland. Geophysical Reseach Letters, 39, L14806.
444
445 Haylock MR, *et al*., 2008: A European daily high-resolution gridded data set of surface
446 temperature and precipitation for 1950–2006, *J. Geophys Res. Atmos*, **113,** D20119.
447
448 Hodges, K. I., 1995: Feature tracking on the unit sphere, *Mon. Wea. Rev*, **123** (12), 3458 –
449 3465.
450
451 Horel, J.D., and J.M. Wallace, 1981: Planetary-Scale Atmospheric Phenomena Associated with
452 the Southern Oscillation, *Mon. Wea. Rev*, **109**, 813 – 829.
453
454 Hoskins, B. J., and P.J. Valdes, 1990: On the existence of storm-tracks, *J. Atmos Sci*, **47** (15),
455 1854 – 1864.
456
457 Kushnir, Y., W.A. Robinson, I. Bladé, N.M.J Hall, S. Peng and R. Sutton, 2002: Atmospheric
458 GCM response to extratropical SST anomalies: Synthesis and evaluation, *J. Climate*, **15** (16),
459 2233 – 2256.
460 Marshall, J., Y. Kushnir, D. Battisti, P.Chang, A. Czaja, R. Dickson, ... and M. Visbeck, 2001:
461 North Atlantic climate variability: phenomena, impacts and mechanisms, *Int. J. Clim*., **21** (15),
462 1863 – 1898.
463
464 Moore, G. W. K. and I. A. Renfrew, 2005: Tip jets and barrier winds: A QuikSCAT climatology
465 of high wind speed events around Greenland, J. Climate, 18, 3713-3725.
466

Rogers, J. C., 1997: North Atlantic storm track variability and its association to the North Atlantic Oscillation and climate variability of northern Europe, *J. Climate*,**10** (7), 1635 – 1647.

Scaife AA, *et al*., 2014: Skillful long-range prediction of European and North American winters, *Geophys. Res. Lett.,* **41**, 2514–2519.

O'Reilly, C. H., J. Heatley, D. MacLeod, A. Weisheimer, T. N. Palmer, N. Schaller, and T. Woollings 2017: Variability in seasonal forecast skill of Northern Hemisphere winters over the twentieth century, Geophys. Res. Lett., 44, 5729–5738, doi:10.1002/2017GL073736.

O'Reilly, C.H., T. Woollings, L. Zanna, and A. Weisheimer, 2018: The Impact of Tropical Precipitation on Summertime Euro-Atlantic Circulation via a Circumglobal Wave Train, *J. Climate,* **31**, 6481 – 6504, https://doi.org/10.1175/JCLI-D-17-0451.1.

Ossó, A., R. Sutton, L. Shaffrey and B. Dong, 2018: Observational evidence of European summer weather patterns predictable from spring, *PNAS,* **115** (1), 59 – 63.

Philander, S. G. H., 1983: El Nino southern oscillation phenomena, *Nature*, **302** (5906), 295.

Rasmusson, E. M., and J.M. Wallace, 1983:. Meteorological aspects of the El Nino/southern oscillation, *Science*, **222**(4629), 1195 – 1202.

Santer B.D., T.M.L. Wigley, J.S. Boyle, D.J. Gaffen, J.J. Hnilo, D. Nychka, D.E. Parker and K.E. Taylor, 2000: Statistical significance of trends and trend differences in layer-average atmospheric temperature time series, *J. Geophys. Res. Atmos.,* **105,** 7337 – 7356.

493 Smith, T. M., R.W. Reynolds, T.C. Peterson, and J. Lawrimore, 2008: Improvements to NOAA's
494 historical merged land–ocean surface temperature analysis (1880–2006), *J. Climate*, **21**(10),
495 2283 –2296.
496
497 Scaife, A. A. et al. (2014): Skilful long range prediction of European and North American
498 winters. Geophys. Res. Lett. 41, 2514–2519.
499
500 Scaife, A. A. and D. Smith, 2018: A signal-to-noise paradox in climate science. *npj Climate*
501 *Atmos. Sci.*, 1, http://dx.doi.org/10.1038/s41612-018-0038-4.
502
503 Webster, P. J., V. O Magana, T. N. Palmer, J. Shukla, R.A. Tomas, M. U. Yanai and T.
504 Yasunari, 1998: Monsoons: Processes, predictability, and the prospects for prediction, *J.*
505 *Geophys. Res. Oce.*,**103** (C7), 14451 – 14510.
506
507 Williams, K. D., C. M. Harris, A. Bodas-Salcedo, J. Camp, R.E. Comer, D. Copsey, ... and P.
508 Hyder, 2015: The met office global coupled model 2.0 (GC2) configuration, *Geos. Mod.*
509 *Develop.*, **8**(5), 1509.
510
511 Wills S.M., D.W.J. Thompson and L.M. Ciasto, 2016: On the Observed Relationships between
512 Variability in Gulf Stream Sea Surface Temperatures and the Atmospheric Circulation in the
513 North Atlantic, *J. Climate,* **29,** 3719 – 3730.
514
515 Woollings, T., A. Hannachi and B. Hoskins, 2010: Variability of the North Atlantic eddy-driven
516 jet stream, *Q. J. R. Meteorol. Soc.*, **136**(649), 856-868.
517

518 Wulff, C. O., R.J. Greatbatch, D.I.V. Domeisen, G. Gollan, and F. Hansen, 2017: Tropical
519 Forcing of the Summer East Atlantic Pattern, *Geophys. Res. Lett*, **115**(8), 1083 – 8.
520
521

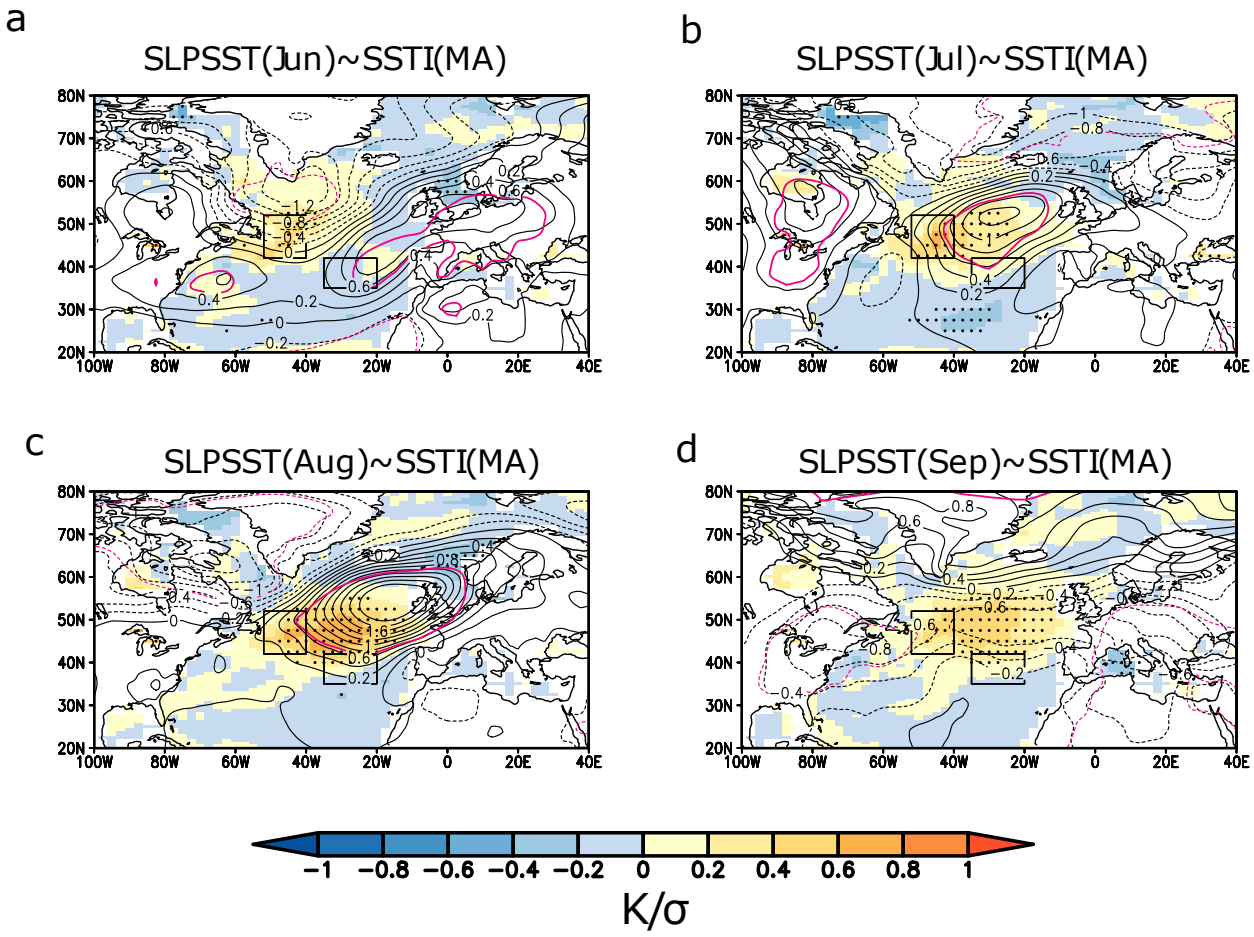

Fig. 1. (a-d) Linear regression maps of the indicated monthly SST (shading) and SLP (contours) anomalies against the precursor MA SST index in ERA-Interim (1979-2017). The SST index is normalized thus the SST and SLP anomalies shown correspond to a standard deviation of the SST index time series. Contour interval is 0.2 hPa σ^{-1}. Stippling indicates SST regression coefficients statistically significant at the 95% confidence level (see section 2). The red contour indicates the critical correlation value between SLP anomalies and the SST index at the 95% confidence level (see section 2). The black boxes indicate the regions used for the SST index, which is calculated as the SST average of the northern box minus the SST average of the southern box.

Accepted for publication in *Journal of Climate*. DOI 10.1175/JCLI-D-19-0613.1.

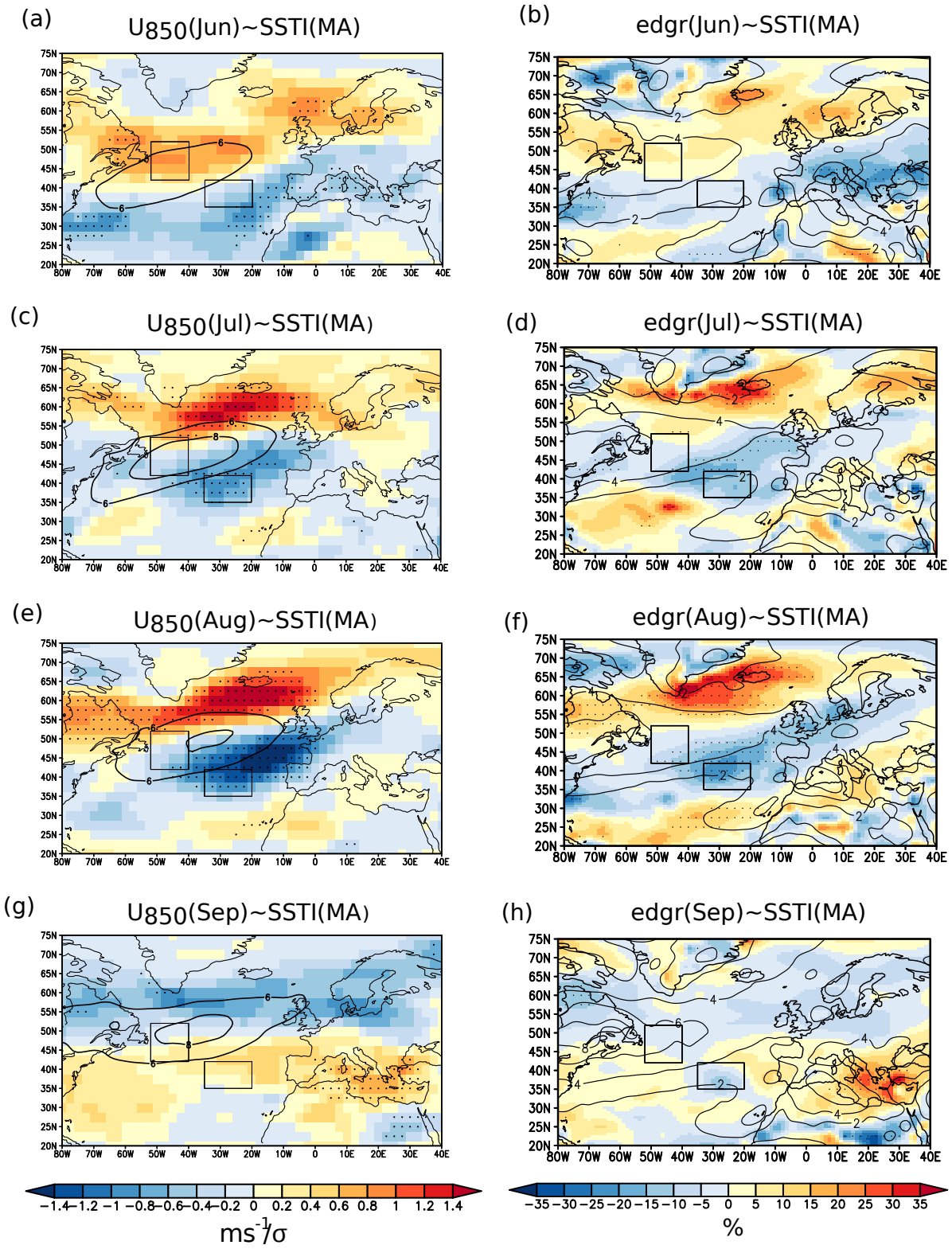

Fig.2 Left column: Linear regression maps of the indicated monthly U_{850} against the precursor MA SST index (shading). The SST index is normalized thus the zonal wind anomalies shown correspond to a standard deviation of the SST index time series. Contours show the corresponding U_{850} climatology (only the largest values are plotted). Stippling indicates U_{850} regression coefficients statistically significant at the 95% confidence level (see section 2). Right column: As in left column, except for eady growth rate (see section 2). The anomalies are expressed as a percentange of its local climatological value. Countours show the corresponding eady growth rate climatology (units: $s^{-1} x10^{6}$).

Accepted for publication in *Journal of Climate*. DOI 10.1175/JCLI-D-19-0613.1.

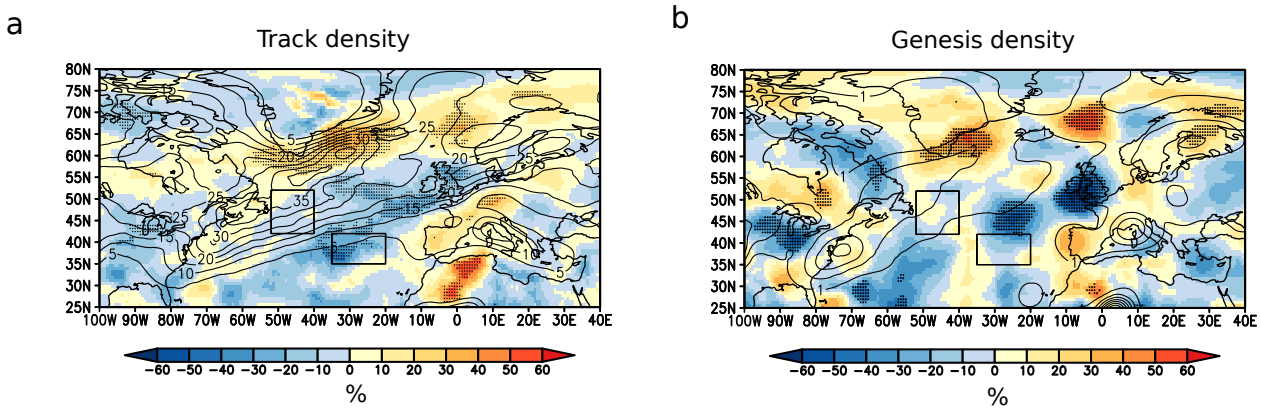

Fig.3 a) Linear regression maps of JA storm track density (a) and genesis density (b) against the MA SST index. The anomaly field is expressed as a percentatge of its local climatological value. Black contours in (a) and (b) are the climatology. Densities are in units of number density per month per unit area, where the unit area is equivalent to a 5° spherical cap ($\sim 10^6$ km^2) (see section 2).

Accepted for publication in *Journal of Climate*. DOI 10.1175/JCLI-D-19-0613.1.

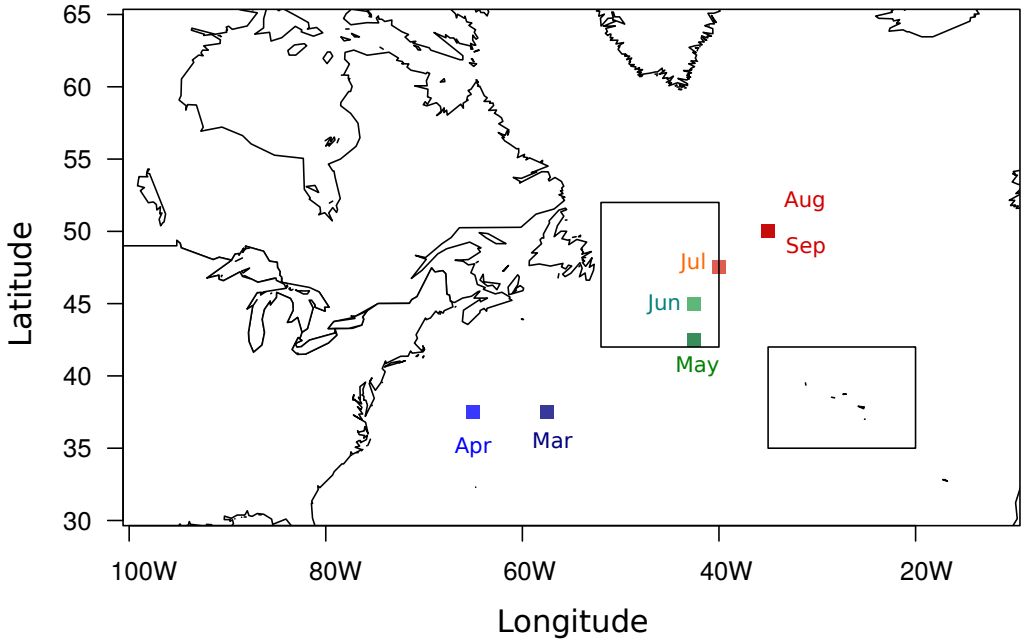

Fig. 4. Seasonal evolution of the geographical position of the North Atlantic eddy-driven jet intensity maximum (see section 2) from March to September.

Accepted for publication in *Journal of Climate*. DOI 10.1175/JCLI-D-19-0613.1.

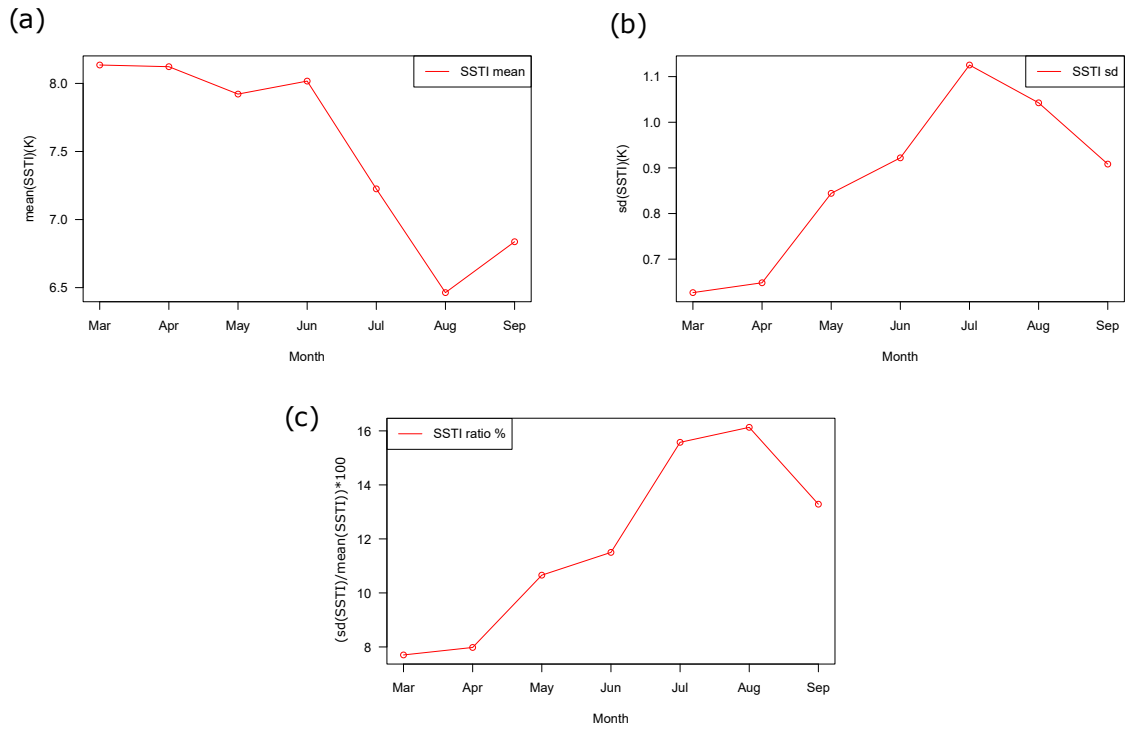

Fig. 5. Seasonal evolution of the monthly SST index (as absolut value (K)) (a), the SST index standard deviation (K) (b) and the ratio between (b) and (a) expressed as a percentatge.

Accepted for publication in *Journal of Climate*. DOI 10.1175/JCLI-D-19-0613.1.

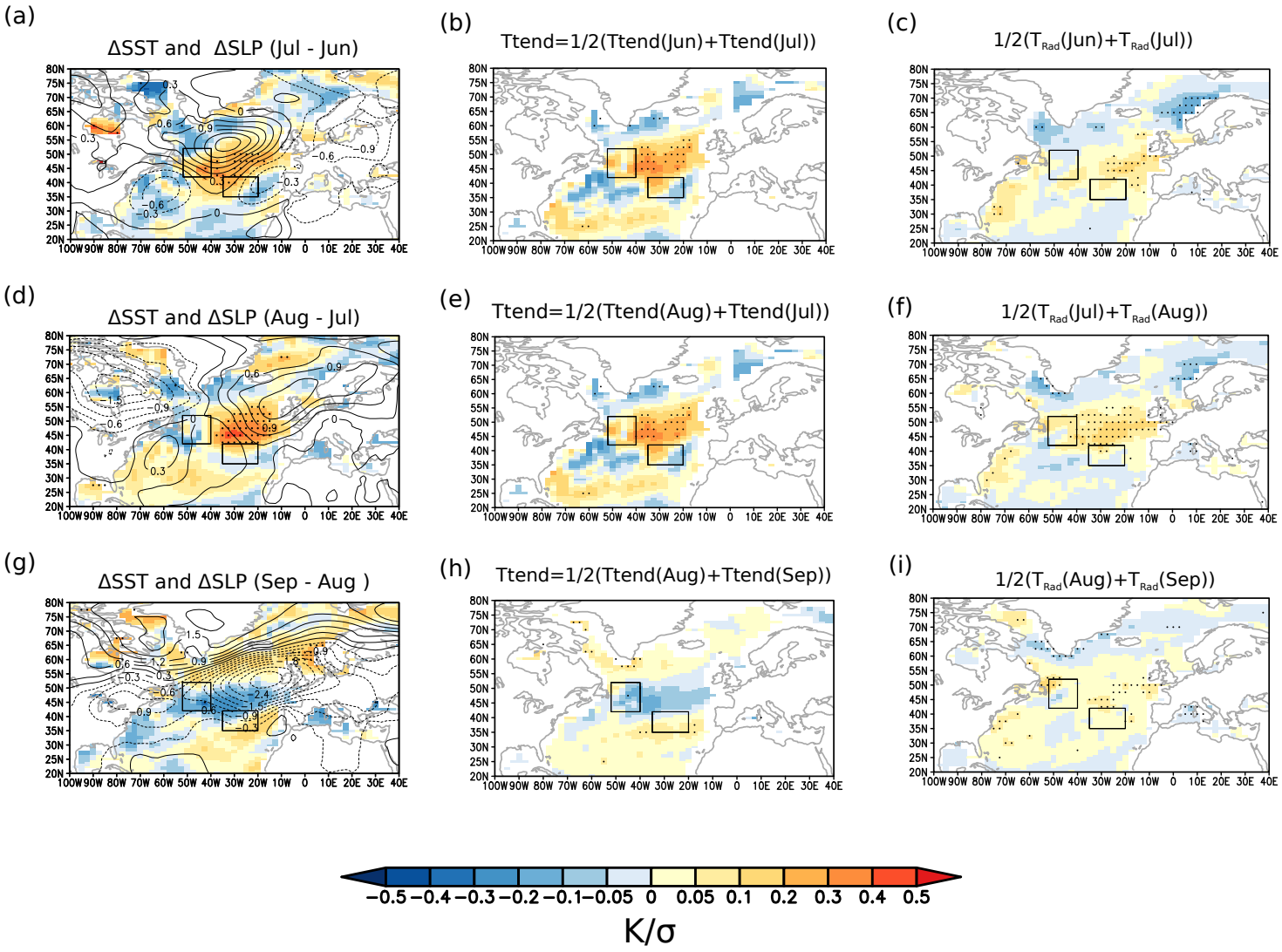

Fig. 6 (a,d,g) Linear regression maps of the SST (shading) and SLP (contours) difference between the months indicated against the MASST index. Contour interval is 0.3 hPa σ^{-1}. (b,e,h) Linear regression maps of the mixed layer ocean temperature tendency (see section 2) for the months indicated against the MA SST index. (c,f,i) As in (b,e,h) but for the temperature tendency due to radiation alone. The MA SST index is normalized thus the anomalies shown correspond to one standard deviation of the MA SST index. Stippling indicates regression coefficients statistically significant at the 95% confidence level (See section 2). The black box indicates the region used to calculate the SST index.

Accepted for publication in *Journal of Climate*. DOI 10.1175/JCLI-D-19-0613.1.

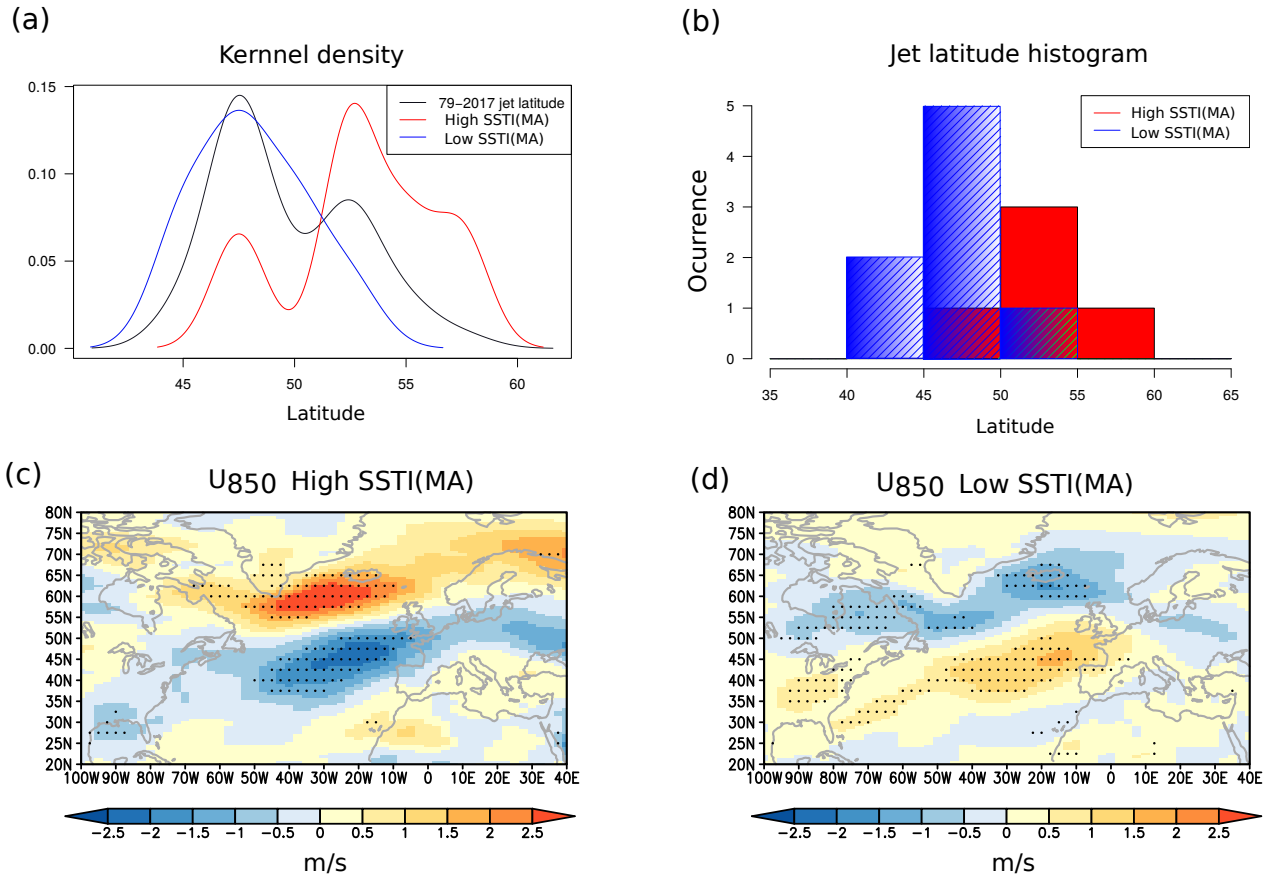

Figure 7: (a) Kernel estimates of the PDF of JA North Atlantic eddy-driven jet latitude in ERA-Interim for the 1979-2017 period (black) and for years with high (red) a low (blue) values of the MA SST Index (See section 2). (b) Distribution of the JA jet stream latitude for high (red) and low (blue) values of the MA SSTI. (c.d) Composites of JA mean U_{850} anomalies for years with high (c) and low (d) values of the MA SSTI. Stippling indicates regions where the composite anomalies are significant at the 95% level estimated using a Monte Carlo resampling method (See section 2).

Accepted for publication in *Journal of Climate*. DOI 10.1175/JCLI-D-19-0613.1.

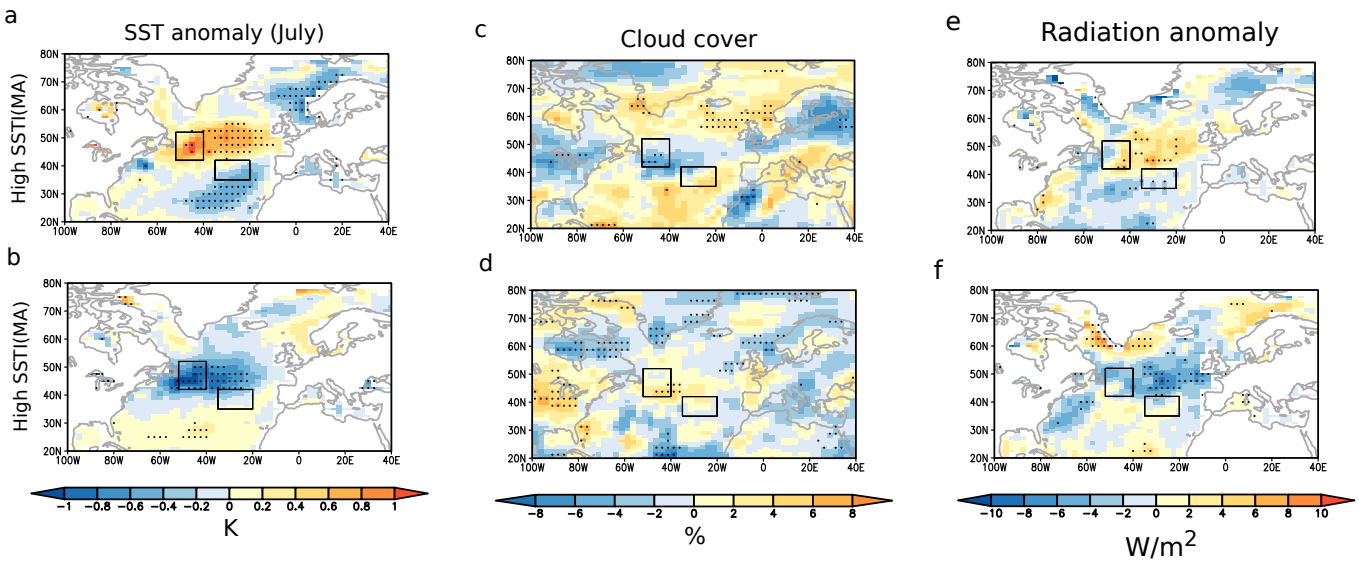

Fig. 8. Upper row: Composites of July SST anomalies (a), cloud fraction (c) and radiation flux (e) for high values of MA SSTI. Bottom row: Same as in upper row except for low values of MA SSTI. Stippling indicates regions where the composite anomalies are significant at the 95% level estimated using a Monte Carlo resampling method (See section 2).

Accepted for publication in *Journal of Climate*. DOI 10.1175/JCLI-D-19-0613.1.

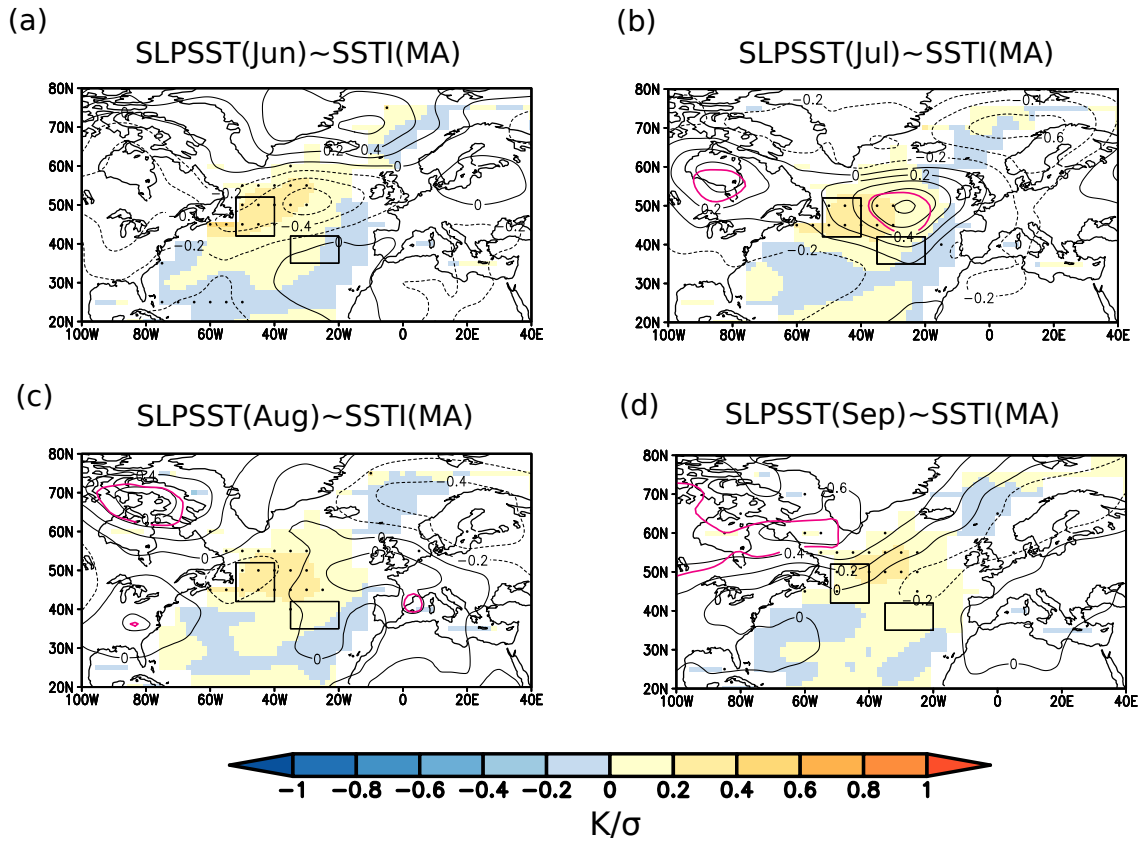

Fig. 9 Same as figure 1 but for 120 years of the GC2 control simulation (See section 2).

Accepted for publication in *Journal of Climate*. DOI 10.1175/JCLI-D-19-0613.1.

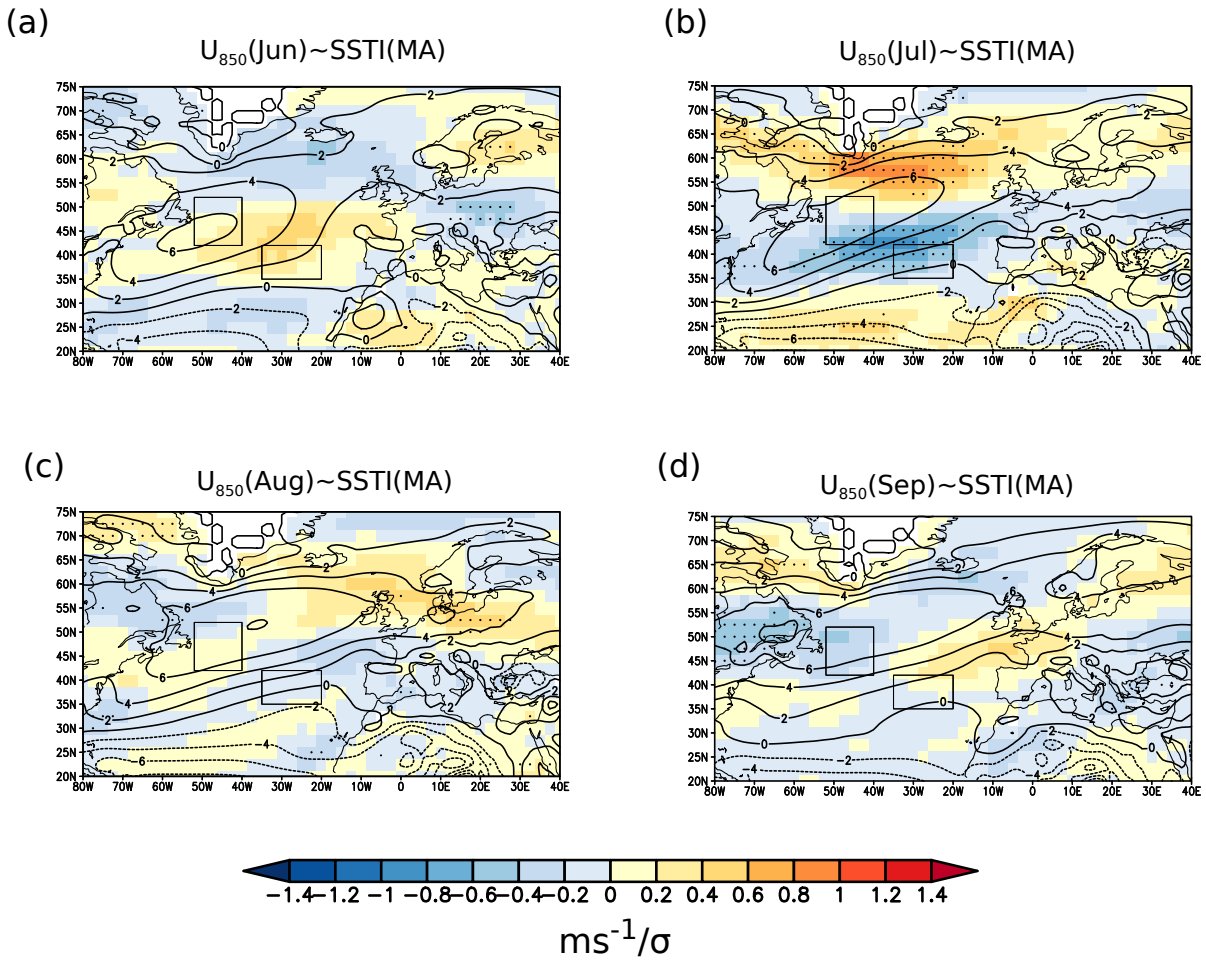

Fig. 10 Same as figure 2a,c,e,g but for 120 years of the GC2 control simulation (See section 2).

Accepted for publication in *Journal of Climate*. DOI 10.1175/JCLI-D-19-0613.1.